JOURNAL OF PROPULSION AND POWER
Vol. 10, No. 6, Nov.–Dec. 1994

High Reynolds Number and Turbulence Effects on Turbine Heat Transfer

Frederick C. Yeh,* Steven A. Hippensteele,* G. James Van Fossen,* and Philip E. Poinsatte†
NASA Lewis Research Center, Cleveland, Ohio 44135
and
Ali Ameri‡
University of Kansas, Lawrence, Kansas 66044

Experimental data on pressure distribution and heat transfer on a turbine airfoil were obtained over a range of Reynolds numbers from 0.75 to 7.0 × 10^6 and a range of turbulence intensities from 1.8 to about 15%. The purpose of this study was to obtain fundamental heat transfer and pressure distribution data over a wide range of high Reynolds numbers and to extend the heat transfer data base to include the range of Reynolds numbers encountered in the Space Shuttle main engine turbopump turbines. The results of this study indicated that Reynolds number and turbulence intensity have a large effect on both the transition from laminar to turbulent flow and the resulting heat transfer. For a given turbulence intensity, heat transfer for all Reynolds numbers at the leading edge can generally be correlated with the Frossling number developed for lower Reynolds numbers. For a given turbulence intensity, heat transfer for the airfoil surfaces downstream of the leading edge can be approximately correlated with a dimensionless parameter. Comparisons of the experimental results were also made with a numerical solution from a two-dimensional Navier-Stokes code.

Nomenclature

A = area, ft^2
B = curve-fitting polynomial coefficient
C = chord length, ft
d = leading-edge diameter, ft
E = mean voltage, V
$Fr(0)$ = Frossling number at stagnation point, $Nu_d/(Re_{inlet})^{0.5}$
h = heat transfer coefficient, Btu/h/ft^2/°F
k = thermal conductivity of air, ≈0.0147 Btu/(h/ft/°F)
L = total length of airfoil pressure or suction surface, in.
Nu_d = Nusselt number based on leading-edge diameter, hd/k
Nu_s = Nusselt number based on distance along airfoil surface from stagnation point, hs/k
P = pressure, psia
Pr = Prandtl number
q = heat flux, Btu/h/ft^2
Re = Reynolds number, based on axial chord and airfoil exit conditions
Re_{inlet} = Reynolds number, based on leading-edge diameter and inlet conditions
r = recovery factor, $(Pr)^{1/3} \approx 0.89$
S = blade pitch, in.
s = distance along airfoil pressure or suction surface from airfoil stagnation point, in.
T = temperature, °R
Tu = turbulence intensity, %
V = fluid velocity, ft/s
W = flow rate, lb/s
θ = flow angle, rad or deg
Λ_x = longitudinal integral length scale
μ = dynamic viscosity, lb/ft·s
ρ = fluid density, lb/ft^3

Subscripts

g = gas
i = input
L = loss
LC = liquid crystal
R = recovery
s = surface distance from airfoil stagnation point
st = static
t = total
0, 1, 2, 3, 4 = curve-fitting polynomial coefficients

Superscript

$'$ = fluctuating velocity component

Introduction

THE turbines used in the Space Shuttle main engine (SSME) run at very high pressures and Reynolds numbers. At these extreme conditions, the heat transfer rates to the turbine airfoils are expected to be significantly higher than those of current aeropropulsion turbines. A detailed knowledge of heat transfer at these extreme conditions is necessary to predict airfoil surface temperatures and satisfy life goals.

A large body of flow and heat transfer data over airfoils for current aeropropulsion turbines at lower Reynolds numbers on the order of 10^6 is available in the literature. However, very little information is available for the range of higher Reynolds numbers found in the SSME turbopump turbines.

A High Reynolds Number Heat Transfer Cascade Facility was constructed at the NASA Lewis Research Center. Its

Presented as Paper 93-2252 at the AIAA/SAE/ASME/ASEE 29th Joint Propulsion Conference and Exhibit, Monterey, CA, June 28–30, 1993; received Sept. 9, 1993; revision received March 9, 1994; accepted for publication March 10, 1994.

*Aerospace Engineer, Heat Transfer Branch, Internal Fluid Mechanics Division.
†Aerospace Engineer, Heat Transfer Branch, Internal Fluid Mechanics Division. Member AIAA.
‡Resident Research Associate, NASA Lewis Research Center. Member AIAA.

purpose was to conduct a fundamental study on heat transfer at Reynolds numbers ranging from current aeropropulsion gas turbine levels to those found in the SSME turbopump turbines. The effect of freestream turbulence on heat transfer and the relationship between heat transfer data at high Reynolds numbers and the current data base was investigated. Turbulence-generating grids were used to vary the turbulence intensity levels in the test section. The facility is capable of operating over a range of Reynolds numbers from 0.75 to over 7.0×10^6 (based on axial chord and airfoil exit conditions) and a range of turbulence intensities from 1.8 to about 15%.

Heat transfer and airfoil pressure distribution data were obtained at Reynolds numbers of 0.75, 1.5, 3.0, 5.0, and 7.0×10^6. The measured turbulence intensity levels ranged from 1.8% at a Reynolds number of 7.0×10^6 with no grid (clear tunnel case) to 15% at a Reynolds number of 0.75×10^6 with $\frac{1}{4}$-in. grid. Preliminary results from this facility were reported by Schobeiri et al.[1] This article presents the latest heat transfer and pressure distribution results from this facility. Experimental heat transfer data are also compared with a numerical solution from a Navier-Stokes code.

Facility

General Description

Figure 1 is an illustration of the test facility, including a cutaway view of the test section. Compressed air at 40 psig and ambient temperature flows through an 18-in.-diam pipe that houses screens and perforated plates for flow conditioning. The maximum flow rate of the facility is about 38 lb/s; the airflow exits to the laboratory exhaust system at 1.93 psia. Upstream of the test section, boundary-layer air is bled from four sides to provide a uniform velocity profile at the test section entrance. The main airflow, as well as each individual bleed airflow, is measured with a sharp-edged orifice.

Test Section

The test section with the cover plate removed is shown in Fig. 2. Visible in this photograph are the airfoil, the contoured sidewalls, the hot film anemometer probe, the inlet and exit flow angle measurement probes, and the pitot static probe. A turbulence grid, not visible, is located behind the grid cover. Two turbulence grids were used to vary the turbulence intensity in the test section. The grids were of the square-mesh, biplane type with square bars: one having $\frac{1}{8}$-in.-square bars and the other having $\frac{1}{4}$-in.-square bars. Tests were also conducted using a clear tunnel only (no grid). The ratio of mesh-to-bar width spacing was 4.5, giving a 60% open flow area. The traversing anemometer probe, mounted on the test section, is located 3.6 leading-edge diam (6.19 in.) downstream from the grid and 0.77 diam (1.31 in.) in front of the airfoil leading edge. The anemometer probe was used to survey the turbulence intensity in the pitchwise direction.

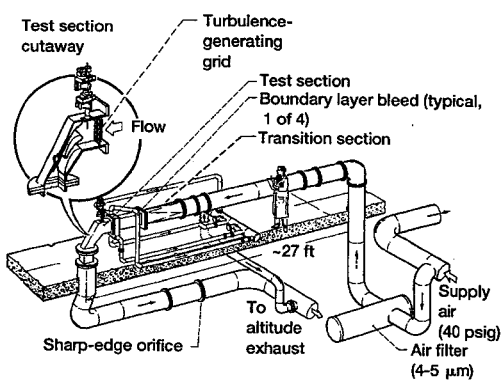

Fig. 1 High Reynolds Number Heat Transfer Facility.

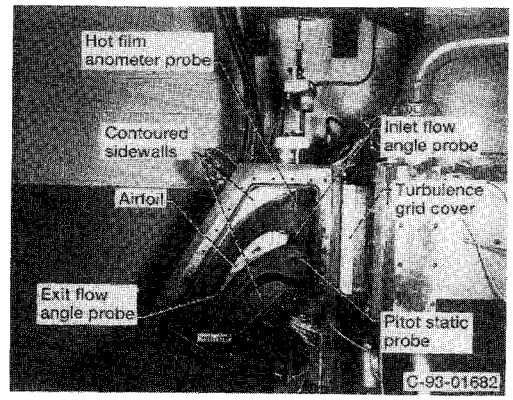

Fig. 2 Test section.

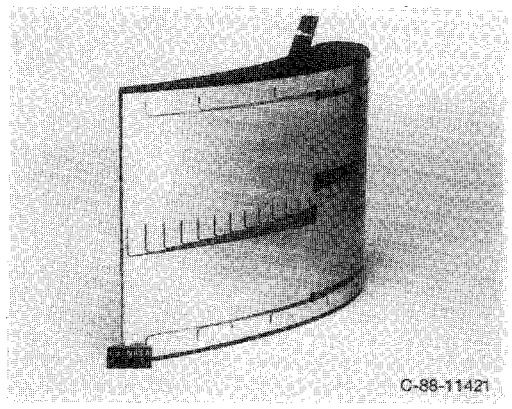

Fig. 3 Pressure distribution airfoil showing pressure tap locations on suction surface.

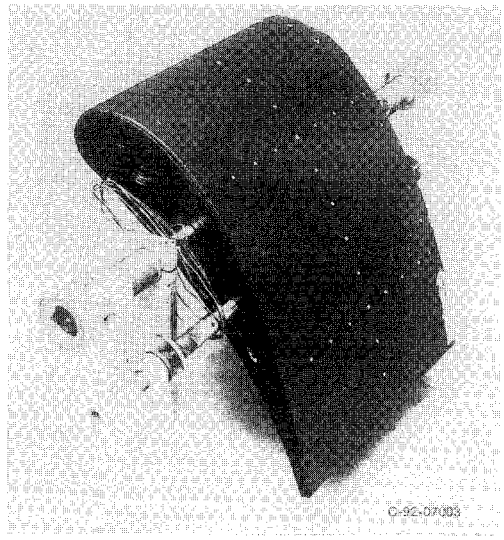

Fig. 4 Heat transfer airfoil showing grid markings for the locations of temperature distribution.

Airfoil

The airfoil used in these tests was an 8X model of the SSME airfoil at midspan. The test airfoil has an axial chord of 8.5 in., a true chord of 11.09 in., a span of 8.5 in., a solidity of 1.32, and a camber angle of 61.7 deg. The airfoil has a constant cross section to provide a uniform flowfield. Coordinates of the airfoil and other geometric information are given in Ref. 1. Two airfoils were fabricated: one was used for pressure distribution tests and the other for heat transfer tests. The pressure distribution airfoil is shown in the photograph of Fig. 3. Of the 90 pressure taps on the airfoil, 52 were located at the midspan, and 19 each were located at the hub and tip

sections to record any three dimensionality of the flowfield around the airfoil.

The airfoil used for heat transfer tests is shown in Fig. 4. It is overlayed with a thin (0.001-in.) Inconel® sheet. Passing an electric current through the Inconel sheet gave a constant heat flux boundary condition. The Inconel sheet was first coated with black paint, then sprayed with a liquid crystal and clear binder mixture. Grid lines were drawn on the airfoil surface to locate the temperature field in the data reduction process. White dots were added as an aid to locate the temperatures indicated by the liquid crystals. Details on the use of the liquid crystal technique on airfoils are given by Hippensteele, Russell, and Torres.[2,3] A thermocouple was also installed on the airfoil to verify the temperature on the Inconel sheet beneath the liquid crystal coating.

Test Procedure

The Reynolds numbers were obtained by varying the inlet flow rate while keeping the inlet pressure approximately constant. Turbulence intensity measurements were obtained by using a constant temperature hot film anemometer, which was installed in a traversing actuator on top of the test section to survey the flow channel in a pitchwise direction at midspan. Heat transfer tests were conducted for Reynolds numbers of 0.75, 1.5, 3.0, 5.0, and 7.0 × 10^6. The inlet Mach numbers ranged from 0.027 to 0.27; exit Mach numbers ranged from 0.058 to 0.71.

Data for turbulence intensity and pressure distribution were first recorded at Reynolds numbers of 0.75, 1.5, 3.0, 5.0, and 7.0 × 10, using the pressure distribution airfoil. The first series of tests were conducted with a clear tunnel (no turbulence grid installed); the second series used the $\frac{1}{8}$-in. grid; and the last series used the $\frac{1}{4}$-in. grid. Because the wide range of flow rates required for the Reynolds numbers tested, two different flow orifices were required for each series: one for Reynolds numbers range from 3.0 to 7.0 × 10^6, and the other for Reynolds numbers of 0.75 and 1.5 × 10^6. The three series of tests for the higher Reynolds number range can be completed in one day. Similarly, tests for the lower Reynolds number range can also be completed in one day. Because of anemometer breakages, time required for orifice change, and other test cell problems, these tests covered a much wider time period. The anemometer was recalibrated before each series of tests.

Heat transfer tests, using the heat transfer airfoil, duplicated the Reynolds number range used for the turbulence and pressure distribution tests. Two orifices were again required to complete the range of flow rates. Because liquid crystal tests require elaborate photographic setups and time for the liquid crystal temperature to attain equilibrium as the power to the liquid crystal is increased,[2,3] these tests require longer facility run time. In general, a complete series of tests for a given orifice size and a given turbulence grid can be completed in one day.

Data Reduction Procedure

Heat Transfer

Surface heat transfer coefficients were obtained from the energy balance

$$h = (q_i - q_L)/(T_{LC} - T_R) \tag{1}$$

where the local heat transfer coefficient h was calculated at the location of the calibrated color band (an isotherm which, in this case, also represents a uniform heat transfer coefficient). The heat flux energy q_i supplied to the Inconel heater sheet at a given color band width was calculated from the measured voltage across the sheet and the current through a shunt resistor in series with the sheet. The heat loss q_L per unit surface at a given color bandwidth was the calculated radiation loss from the surface. The very low thermal conductivity material used for the airfoil makes interior heat conduction loss negligible, and thus it is neglected. The temperature of the test surface T_{LC} was the calibrated liquid crystal temperature. The local recovery temperature T_R of the freestream air around the airfoil was calculated as

$$T_R = T_{st} + r(T_t - T_{st}) \tag{2}$$

where T_t is the freestream total temperature, T_{st} is the local static air temperature around the airfoil, and r is the recovery factor, defined as the cube root of the Prandtl number. The static air temperature around the airfoil is computed from the "Ames Tables,"[4] the Mach numbers around the airfoil being obtained from the measured freestream total pressure and the static pressures around the airfoil. The difference between the recovery temperature and the liquid crystal temperature is dependent upon the Reynolds number and the location where the temperature is measured. At the stagnation point, the difference is zero. At the trailing edge, the difference is in the order of 50°F at Reynolds number of 7.0 × 10^6, and less than 1°F at Reynolds number of 0.75 × 10^6.

Reynolds Number Measurement

The Reynolds number is based on the axial chord and the exit conditions

$$Re = C(\rho V)_{exit}/\mu \tag{3}$$

where $(\rho V)_{exit} = W/A_{exit}$, and

$$A_{exit} = S \cos \theta \tag{4}$$

In this article, the flow angle is taken as equal to the camber angle (61.7 deg), which is approximately the case for subsonic flow. W is measured by a sharp-edged orifice downstream of the test section.

Turbulence Measurements

Turbulence intensity was measured with a TSI model 1210-20 hot film probe, located 6.19 in. downstream of the turbulence grid. Flow was normal to the probe axis. The probe was calibrated in the tunnel, upstream of the turbulence grid and boundary-layer bleeds, by varying the Reynolds number over the range used in this study. The probe voltage was plotted against the calculated density-velocity product, and a fourth-order, least-squares curve fit was obtained

$$\rho V = B_0 + B_1 E + B_2 E^2 + B_3 E^3 + B_4 E^4 \tag{5}$$

where ρV is the density-velocity product, and E is the mean voltage read from an integrating voltmeter. The turbulence intensity was then obtained from the calibration curve as

$$Tu = \frac{\rho V'}{\rho V} = \frac{d[\rho V(E)]}{dE} \frac{dE}{\rho V(E)} \tag{6}$$

where dE is taken as the rms of the fluctuating voltage read from a true rms meter. The turbulence intensity was measured in midchannel because it represented the location in the flow channel least affected by the airfoil leading edge and the sidewall. As a check on Eq. (6), E and the rms of the fluctuating voltages dE were recorded on a strip chart for each Reynolds number as the anemometer probe was traversed across the flow stream in a pitchwise direction at midspan.

Results and Discussion

Figure 5 presents turbulence intensities as a function of Reynolds number for three test conditions: clear tunnel (no grid), $\frac{1}{8}$- and $\frac{1}{4}$-in. grids. In general, the turbulence intensities show a stronger Reynolds number dependency at lower Reynolds numbers. In all cases, the turbulence intensities de-

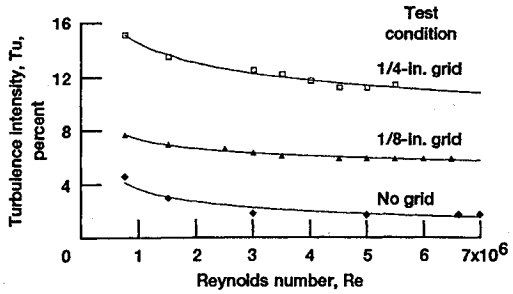

Fig. 5 Turbulence intensity as a function of Reynolds number for three test conditions.

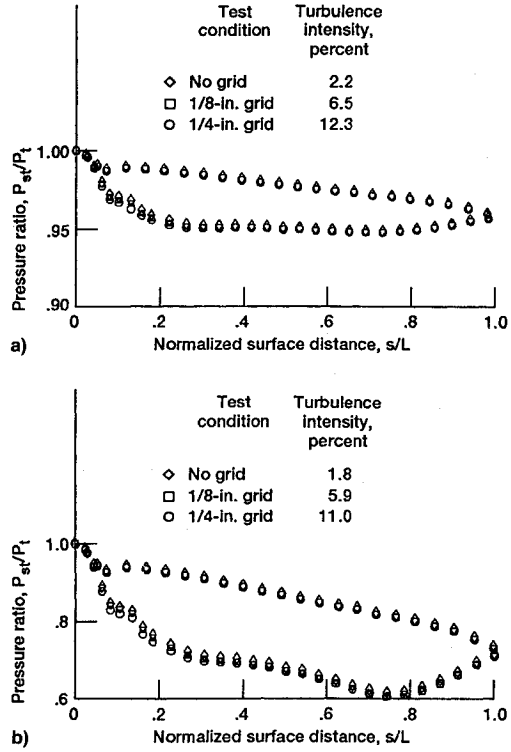

Fig. 6 Effect of turbulence intensity on airfoil pressure distribution at midspan. Re = a) 3.0 × 10⁶ and b) 7.0 × 10⁶.

creased only slightly for Reynolds numbers greater than 3.0 × 10⁶. The turbulence intensities for the clear tunnel (no grid) shown here are higher than those obtained from a typical quiescent wind tunnel because of the turbulent pipe flow condition that exists ahead of the test section. For the cases of the ⅛- and ¼-in. bar grids, the turbulence intensities are in general agreement with those calculated from Baines and Peterson[5] for Reynolds numbers greater than 3.0 × 10⁶.

Pressure Distribution

Both the airfoil and the contoured sidewalls were instrumented with the same number of pressure taps to check the effect of periodicity, as well as the three dimensionality, of the flow in the cascade.

Figures 6a and 6b show the effect of turbulence intensity on the airfoil pressure distribution at midspan at Reynolds numbers of 3.0 and 7.0 × 10⁶, respectively. The turbulence levels varied from 12.3 to 1.8% depending on the Reynolds numbers and the turbulence grids used in these tests. The figures indicated that turbulence intensity has little or no effect on the airfoil pressure distribution. The turbulence intensity effects at other Reynolds numbers are also negligible. Similar plots for the airfoil hub and tip regions of the present experiment also show little or no turbulence intensity dependency on pressure distribution. These findings are in general agreement with Dring et al.,[6] who reported on the aerodynamic

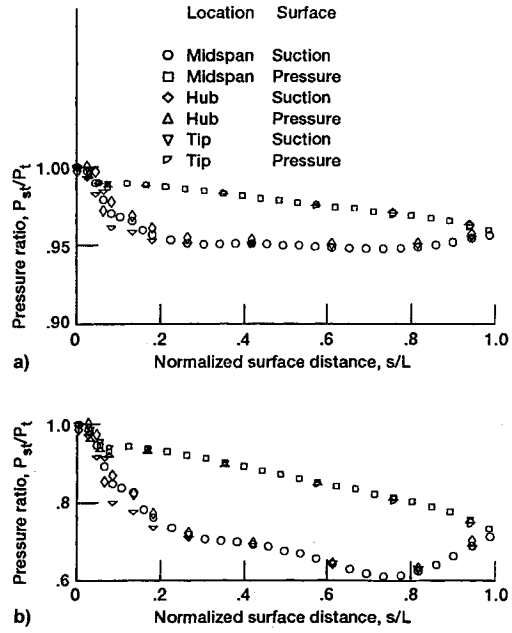

Fig. 7 Airfoil pressure distribution at midspan, hub, and tip: a) Re = 3.0 × 10⁶, ⅛-in. grid, turbulence intensity, 6.5% and b) Re = 7.0 × 10⁶, ⅛-in. grid, turbulence intensity, 5.9%.

and heat transfer characteristics of a large-scale rotating turbine model. They found that the midspan pressure distributions were essentially unaffected by the turbulence generating grid.

Figure 7a compares the airfoil pressure distribution at the hub, midspan, and tip for a Reynolds number of 3.0 × 10⁶ and a turbulence intensity of 6.5% (⅛-in. grid). The figures show that, except near the suction surface leading edge, there is no variation in the spanwise pressure distribution. This is an indication that the flow on the airfoil is mostly two dimensional. Similar results are noted in Fig. 7b for a Reynolds number of 7.0 × 10⁶ and a turbulence intensity of 5.9%.

For the ⅛-in. grid case, Figs. 8a–8c compare the pressure distribution between the airfoil and the contoured sidewall at midspan for Reynolds numbers of 3.0, 5.0, and 7.0 × 10⁶. The agreement between the airfoil and the contoured sidewall is good on the pressure surface for all the Reynolds numbers shown. For the suction surface, the agreement is also good for about 50% of the airfoil. From about 50% of the chord to the trailing edge there is deviation between the airfoil and sidewall pressure distribution. The deviation increases progressively with Reynolds number. The deviation is especially obvious at a Reynolds number of 7.0 × 10⁶. It is speculated here that the reason for the deviation at the suction surface near the trailing edge is that the facility is not a true cascade. In a true cascade, the airfoil suction surface would be uncovered downstream of the throat. In this facility the continuation of the contoured sidewall pressure surface that forms the cascade wall would cause the air to continue to accelerate downstream of the throat, thereby causing the pressure to decrease. This effect is seen at all Reynolds numbers; however, it was especially pronounced at Re = 7.0 × 10⁶.

Heat Transfer

In Fig. 9a the heat transfer coefficient is plotted against the normalized surface distance s/L for Reynolds numbers of 0.75, 1.5, 3.0, 5.0, and 7.0 × 10⁶ for the clear tunnel (no grid) case. As seen in the figure, heat transfer increases with Reynolds number, as expected. On the pressure surface, the transition (as evidenced by the sharp rise in the heat transfer coefficient) appears to occur near an s/L of 0.09, which is near the point of tangency of the leading-edge circle. Examination of the liquid crystal photographs reveals the presence of a weak separation at this point. The pressure distribution contour also

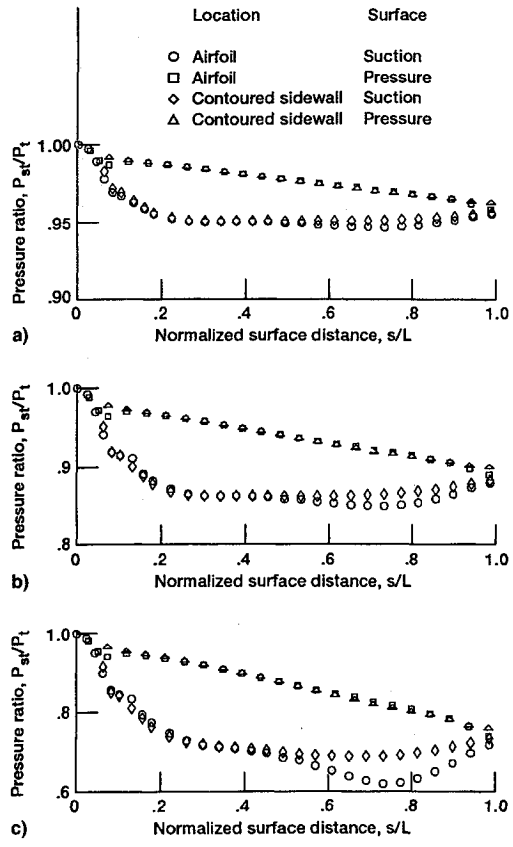

Fig. 8 Comparison of airfoil and contoured sidewall pressure distribution at midspan for $\frac{1}{8}$-in. grid: a) $Re = 3.0 \times 10^6$, turbulence intensity, 6.5%; and b) $Re = 5.0 \times 10^6$, turbulence intensity, 6.1%; and c) $Re = 7.0 \times 10^6$, turbulence intensity, 5.9%.

indicates a small adverse gradient near this region. It is speculated that flow separation at this point triggers the transition for the three highest Reynolds numbers; this is the reason why the transition point does not change with increasing Reynolds number. After the initial rise due to transition, the heat transfer coefficient continues to increase at a reduced rate; this is caused by the flow acceleration on the pressure surface.

On the suction surface, the location of the transition moves upstream with increasing Reynolds numbers, indicating that no flow separation is present. This is supported by the fact that the pressure distribution on the suction surface does not show any adverse pressure gradient and that the liquid crystal photographs do not show evidence of flow separation.

Near the suction surface trailing edge, the heat transfer coefficient for a Reynolds number of 7.0×10^6 shows an increasing trend, which is incompatible with the increase in static pressure and the corresponding decrease in flow velocity in this region as shown in Fig. 8c. The reason for this anomaly is not known at this time.

Figures 9b and 9c present the heat transfer coefficients for the moderate and high turbulence cases ($\frac{1}{8}$- and $\frac{1}{4}$-in. grids). On the pressure surface, the separation at $s/L = 0.09$ is still present and can be seen as a small dip in the heat transfer coefficient at the two lowest Reynolds numbers. As the Reynolds number is increased, the transition moves upstream from this point. For the two highest Reynolds numbers, there is an abnormal drop in the heat transfer coefficient at the end of the transition region that corresponds to the separation point. This drop was also observed by Hippensteele.[3]

In comparison with Fig. 9a for the clear tunnel case, heat transfer for the suction surface and at the leading-edge region is higher because of the higher turbulence intensity resulting from the $\frac{1}{8}$- and $\frac{1}{4}$-in. grids used. Also, transition from laminar to turbulent flow occurs sooner and over shorter distances.

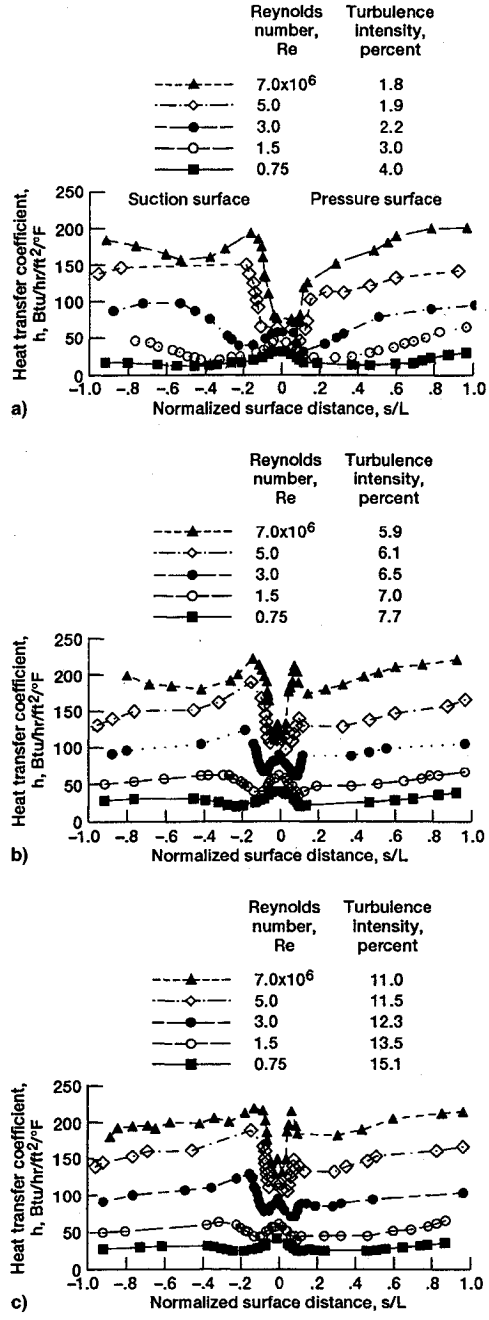

Fig. 9 Effect of Reynolds number on heat transfer coefficient: a) no grid, b) $\frac{1}{8}$-in. grid, and c) $\frac{1}{4}$-in. grid.

For the same reason, heat transfer for both the pressure and suction surfaces is also higher than that for the clear tunnel case. These trends were also noted by Dring et al.[6]

At the leading edge, where the flow is laminar, heat transfer varies as $Re^{0.5}$. At low turbulence levels and low Mach numbers, a plot of the Frossling numbers $[Nu_d/(Re_{inlet})^{0.5}]$ should fall on the same curve. Figure 10a is a plot of the Frossling numbers at the leading-edge region for the clear tunnel case. At Reynolds numbers of 0.75 and 1.5×10^6, the Frossling numbers in the leading-edge region do generally fall on a single curve. At Reynolds numbers of 5.0 and 7.0×10^6, the Frossling numbers deviate considerably from those shown for the lower Reynolds numbers. The reason why some Frossling numbers are lower is not known at this time.

As the flow departs from laminar behavior, heat transfer no longer varies as the square root of Reynolds number, and the Frossling correlation is no longer valid. In regions where the flow is turbulent, Fig. 10a shows that as the Reynolds number is increased the transition from laminar to turbulent

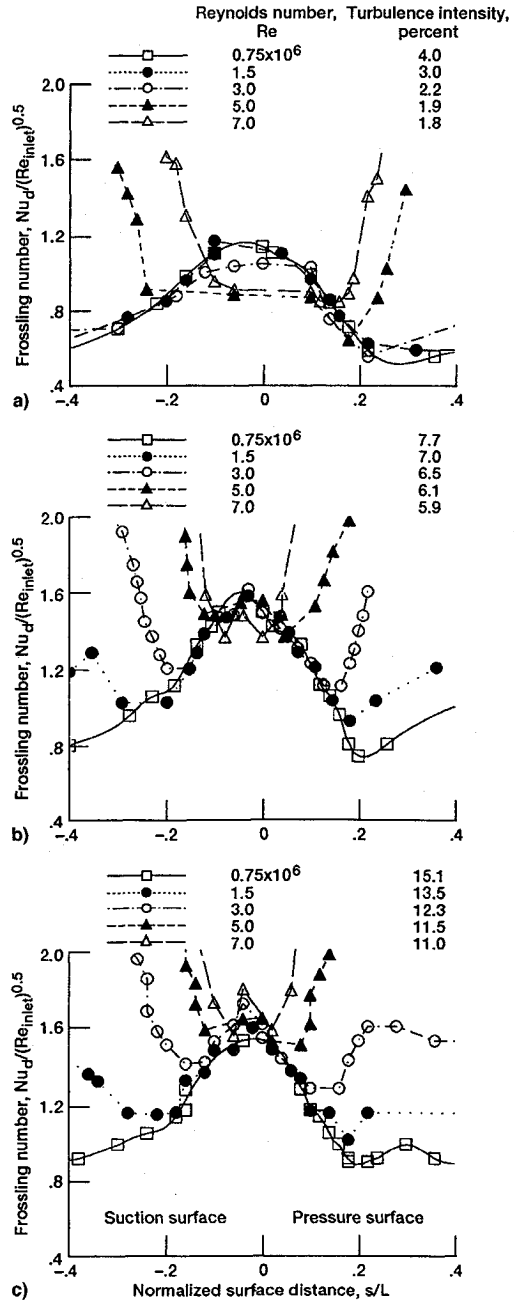

Fig. 10 Frossling correlation of high Reynolds number heat transfer data at leading edge: a) no grid, b) $\frac{1}{8}$-in. grid, and c) $\frac{1}{4}$-in. grid.

flow occurs progressively nearer to the stagnation point. The range of s/L shown in Fig. 10 is extended beyond the valid range of the Frossling correlation length scale (leading-edge diameter d) to indicate the transition from laminar to turbulent flow in the leading-edge region as a function of Reynolds number.

Figure 10b shows Frossling numbers with moderate turbulence intensity ($\frac{1}{8}$-in. grid) upstream of the vane. Frossling numbers for the leading-edge region generally fall on a single curve except at Reynolds number of 7.0×10^6. Compared to Fig. 10a, Fig. 10b shows that transition from laminar to turbulent flow occurs sooner, especially for those at higher Reynolds numbers. Because the stagnation region heat transfer is augmented by higher freestream turbulence intensity, the level of this curve is higher than that of Fig. 10a.

Figure 10c shows Frossling numbers for the high turbulence intensity ($\frac{1}{4}$-in. grid) case upstream of the vane. There is greater data scatter shown on this plot. Transition from laminar to turbulent flow occur sooner than the moderate turbulent intensity ($\frac{1}{8}$-in. grid) case. At Reynolds number of 7.0×10^6,

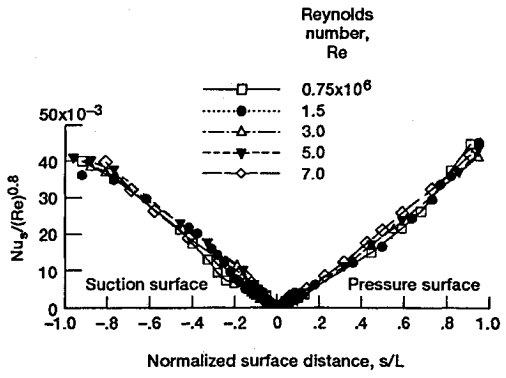

Fig. 11 Correlation of high Reynolds number heat transfer data for $\frac{1}{8}$-in. case.

transition occurs almost immediately aft of the stagnation point.

It would be reasonable to raise the question that if laminar heat transfer at the leading edge with similar turbulence intensity levels can generally be normalized by the Frossling number, is it possible—for similar turbulence intensities—to normalize the turbulent heat transfer for the remaining airfoil surfaces? One possible approach would be to use the Nusselt number (based on the distance from the stagnation point) divided by the Reynolds number (based on the axial chord and exit conditions) raised to the 0.8 power $[Nu_s/(Re)^{0.8}]$. Such an attempt was made using data from the $\frac{1}{8}$-in. grid (see Fig. 11). In this figure, heat transfer values at the leading edge should be disregarded because the plotting parameter is not valid for the leading-edge area. For the remaining airfoil surfaces, the figure shows a data spread of approximately $\pm 6\%$ on both the suction and pressure surface trailing edges. The data spread is larger near the transition region because transition occurs at different locations and over different transition lengths at different Reynolds numbers.

It is hypothesized that there are two reason for the good correlation shown in Fig. 11:

1) The correlating parameter $Nu_s/(Re)^{0.8}$ is basically a flat plate correlation for turbulent flow. Aft of the leading edge, heat transfer on the airfoil surface approaches the flat plate solution.

2) Because of the high Reynolds numbers used in these tests, the flow became turbulent for most of the leading-edge region.

It may be concluded from the foregoing discussions that, for similar turbulence intensities, heat transfer for high Reynolds numbers at the leading edge can be approximately correlated by using the Frossling equation developed for lower Mach numbers. For the rest of the airfoil, heat transfer for similar turbulence intensities may be approximately correlated by using the parameter $Nu_s/(Re)^{0.8}$.

Figure 12a compares the effect of turbulence intensity at Re numbers of 0.75×10^6 for the clear tunnel, $\frac{1}{8}$- and $\frac{1}{4}$-in. grid cases, respectively. The increase in stagnation region heat transfer from the clear tunnel to the $\frac{1}{8}$-in. grid (higher levels of turbulence) case is very evident. However, there seemed to be no difference between the $\frac{1}{8}$- and $\frac{1}{4}$-in. grid cases at the leading-edge region. The fact that the heat transfer coefficient for the $\frac{1}{8}$- and the $\frac{1}{4}$-in. grid cases falls on the same curve is somewhat unexpected, considering the $\frac{1}{8}$-in. grid produces a turbulence level of about 6% and the $\frac{1}{4}$-in. grid about 11%. The reason for this result is not known, but it could possibly be attributed to the larger turbulent integral length scale for the $\frac{1}{4}$-in. grid. The heat transfer coefficient in the stagnation region is proportional to the turbulence intensity, and it has been shown to be inversely proportional to the ratio of the integral length scale to the leading-edge diameter by Van Fossen and Ching.[7] The figure also shows that higher turbulence levels move transition further upstream.

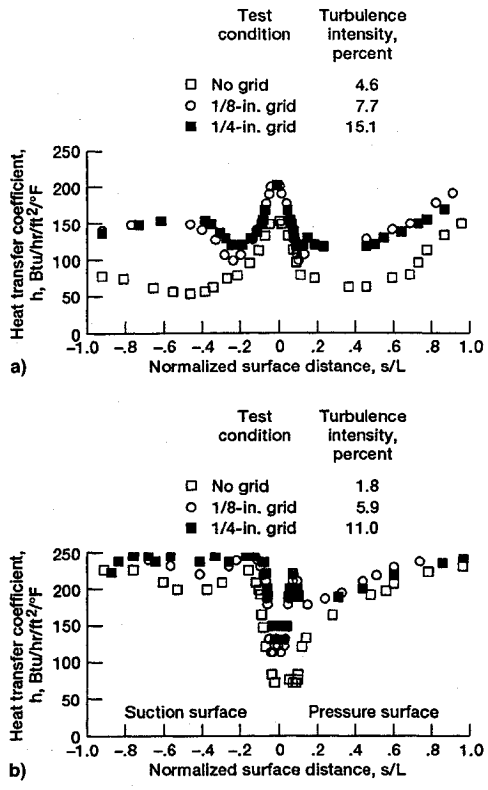

Fig. 12 Effect of turbulence intensity on heat transfer coefficient. *Re* = a) 0.75 × 10⁶ and b) 7.0 × 10⁶.

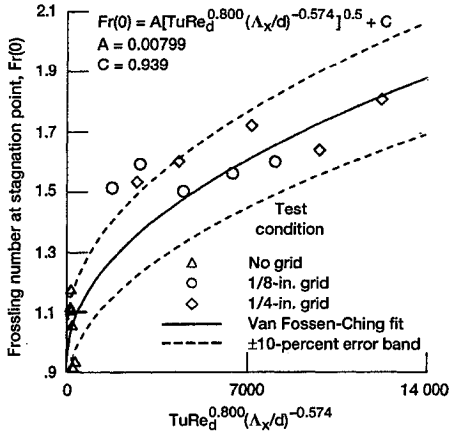

Fig. 13 Heat transfer at stagnation point.

Figure 12b compares the effect of turbulence intensity at $Re = 7.0 \times 10^6$. At this high Reynolds number, the transition point has moved upstream almost to the stagnation point. The heat transfer coefficients for the $\frac{1}{8}$-in. grid are still higher than those for the clear tunnel (no grid), but the heat transfer coefficients for the $\frac{1}{8}$- and the $\frac{1}{4}$-in. grid cases are no longer coincident in the stagnation region; the $\frac{1}{4}$-in. grid has the highest heat transfer coefficients there.

In Fig. 13 the Frossling number at the stagnation point is plotted against a parameter developed by Van Fossen and Ching. This parameter involves turbulence intensity, Reynolds number, and integral length scale. The solid curve is their correlation and the dashed curve is a ±10% error band. Integral length scales for the present data were estimated from Van Fossen and Ching's curve fit of the integral length scale vs the distance; they used $\frac{1}{2}$-, $\frac{1}{4}$-, $\frac{1}{8}$-, and $\frac{1}{16}$-in. grids that had the same ratio of bar width to mesh spacing as that of the present test. For the data with clear tunnels (no grid), the integral length scale was set to the width of the test section, 8.5 in. Agreement with the correlation is reasonable, especially at the high Reynolds numbers for the two turbulence

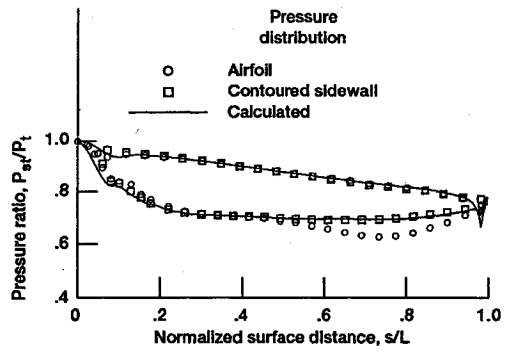

Fig. 14 Comparison of computed and experimental pressure distribution of airfoil and contoured sidewall at Reynolds number of 7.0 × 10⁶.

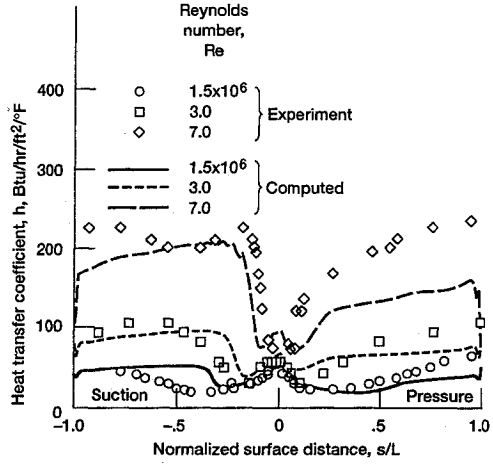

Fig. 15 Comparison of computed and experimental airfoil heat transfer coefficients for clear tunnel (no grid) condition.

grids. Agreement for the clear tunnel case is not quite as good, but is still reasonable considering the greater uncertainty in the length scale used.

Figure 14 compares the pressure distributions of the airfoil and the contoured sidewall at $Re = 7.0 \times 10^6$ with the computed pressure distribution from the TRAFC2D[8] (TRAnsonic Flow 2D) code. The predicted values agree well with the contoured sidewall experimental data, except that near the suction surface leading-edge area. The small disagreement on the suction surface leading-edge area is probably caused by the three-dimensional effect. Because the code used was a two-dimensional version, it was not able to follow the three-dimensional pressure distribution. The agreement is good for the rest of the contoured sidewall data. The airfoil pressure on the suction surface near the trailing edge decreased because of the presence of the contoured sidewall (see the earlier discussion in the Pressure Distribution section).

A comparison of the predicted and experimental heat transfer coefficients is presented in Fig. 15 for Reynolds numbers of 1.5, 3.0, and 7.0 × 10⁶ for the clear tunnel case. The TRAF2D code, described by Arnone et al.,[8] uses a cell-centered finite volume approach. The governing equations solved are the conservative form of Reynolds-averaged Navier-Stokes equations in a curvilinear coordinate system in terms of the Cartesian components of velocity and specific total energy. The perfect gas law is used as the equation of state. The equations are solved using a four-stage Runge-Kutta time-stepping method. To accelerate convergence, the code employs the full approximation storage (FAS) multigrid method originally devised by Brandt[9] and Jameson.[10] Variable coefficient implicit smoothing of the residuals is performed to further increase the rate of convergence. Eigenvalue scaling of the artificial dissipation terms first devised by Martinelli[11]

is adopted to prevent odd-even decoupling and to capture shocks. A C-type grid developed by Arnone et al.,[8] which uses unequal number of grid points on the pressure side and on the suction side of the blade is employed for discretization of the flowfield. The pitchwise grid is constructed first by generating an inviscid grid using an elliptic procedure. The viscous grid is then made by embedding grid lines in the vicinity of the no-slip boundaries with the desired wall spacing. For the present calculations, grid densities of 321 × 49 and 321 × 65 in the streamwise and blade-to-blade directions is employed. The finer grid was used for the calculations at the highest Reynolds number. Periodicity is assumed in the blade-to-blade direction. The inlet boundary condition to the computational domain is set by specifying the values of total temperature, total pressure, and flow angle, and extrapolating all other variables to the inlet boundary from inside the computational domain. At the exit, the pressure is specified and the remaining variables are set by extrapolation. For the present calculations, the Baldwin-Lomax[12] algebraic turbulence model has been employed. The laminar-turbulent is handled by assuming bypass transition, and employing Mayle's[13] model for the start and duration of transition. As can be seen from the figure, the heat transfer coefficients on the suction surface are relatively well predicted. On the pressure surface, the heat transfer coefficients are underpredicted for all the Reynolds numbers. The predicted heat transfer values show encouraging results; however, it is evident that additional work on the predictive techniques is required.

Uncertainty Analysis

An uncertainty analysis, based on the work of Abernathy and Benedict,[14] showed that the uncertainty is a function of Reynolds numbers. For all Reynolds numbers and all turbulence levels tested in this facility, a conservative estimate of the uncertainty of the heat transfer coefficients is approximately 6%, with the exception of two cases (Re = 3.0 and 5.0 × 10^6, for the clear tunnel). The uncertainty of the heat transfer coefficients for these two worst cases is 11 and 8.7%, respectively. The high uncertainty level of these two cases is attributed to the extremely warm air temperature in these tests (91°F), resulting in a temperature difference of only 10°F between the air and the liquid crystal.

Conclusions

Aerodynamic and heat transfer data were presented for Reynolds numbers ranging from 0.75 to 7.0 × 10^6, and turbulence intensities ranging from 1.8 to 15.1%. The range of Reynolds numbers encompassed those encountered in current aeropropulsion turbines and in the SSME turbopump turbines.

From the pressure distribution plots presented, the following can be concluded:

1) The flow in the cascade was nonperiodic at the airfoil suction surface near the trailing edge. This nonperiodicity was evident in all Reynolds numbers, although it was not very pronounced except at Re = 7.0 × 10^6.

2) The flow over the airfoil was primarily two dimensional.

3) The turbulence intensity had a minimal effect on the pressure distribution, as expected.

4) A numerical solution using the TRAFC2D code for pressure distribution agreed well with the contoured sidewall data.

With respect to heat transfer, the results of this study indicated the following:

1) For the high Reynolds numbers typical of the SSME turbopump, heat transfer was dominated by transitional and turbulent flow downstream of the stagnation region.

2) For a given turbulence intensity level, heat transfer at the leading edge for all Reynolds numbers can generally be correlated with the Frossling number developed for lower Reynolds numbers.

3) For a given turbulence intensity, heat transfer on the airfoil downstream of the leading edge can be approximately correlated by using a dimensionless parameter (Nusselt number, based on the distance from the stagnation point, divided by the Reynolds number, based on the axial chord and exit conditions, raised to the 0.8 power) to within ±6% at the trailing edge.

4) A comparison of the experimental heat transfer data with the numerical solution of the TRAFC2D code showed encouraging results.

References

[1]Schobeiri, T., McFarland, E. R., and Yeh, F. C., "Aerodynamic and Heat Transfer Investigations on a High Reynolds Number Turbine Cascade," American Society of Mechanical Engineers Paper 91-GT-157, June 1991.

[2]Hippensteele, S. A., Russell, L. M., and Stepka, F. S., "Evaluation of a Method for Heat Transfer Measurements and Thermal Visualization Using a Composite of a Heater Element and Liquid Crystals," *Journal of Heat Transfer*, Vol. 105, No. 1, 1983, pp. 184–189; also NASA TM-81639, April 1981.

[3]Hippensteele, S. A., Russell, L. M., and Torres, F. J., "Use of a Liquid-Crystal, Heater Element Composite for Quantitative, High Resolution Heat Transfer Coefficients on a Turbine Airfoil, Including Turbulence and Surface Roughness Effects," *Pressure Temperature Measurements*, edited by J. H. Kim and R. J. Moffat, American Society of Mechanical Engineers, New York, 1987, pp. 105–120; also NASA TM-87355, May 1987.

[4]Ames Research Staff, "Equations, Tables, and Charts for Compressible Flow," NACA Rept. 1135, 1953.

[5]Baines, W. D., and Peterson, E. G.,"An Investigation of Flow Through Screens," *Transactions of the American Society of Mechanical Engineers*, Vol. 72, July 1951, pp. 468–480.

[6]Dring, R. P., Blair, M. F., Joslyn, H. D., Power, G. D., and Verdon, J. M., "The Effects of Inlet Turbulence and Rotor/Stator Interactions on the Aerodynamics and Heat Transfer of a Large-Scale Rotating Turbine Model," Vol. 1, NASA CR-4079, May 1986.

[7]Van Fossen, G. J., and Ching, C. Y., "Measurements of the Influence of Integral Length Scale on Stagnation Region Heat Transfer," 5th International Symposium on Transport Phenomena and Dynamics of Rotating Machinery, Paper TP-16, Kaanapali, HA, May 1994; also NASA TM 106503, Feb. 1994.

[8]Arnone, A., Liou, M. S., and Povinelli, L. A., "Navier-Stokes Solution of Transonic Cascade Flow Using Non-Periodic C-Type Grids," *Journal of Propulsion and Power*, Vol. 8, No. 2, 1992, pp. 410–417.

[9]Brandt, A., "Multi-Level Adaptive Computations in Fluid Dynamics," AIAA Paper 79-1455, July 1979.

[10]Jameson, A., "Transonic Flow Calculations," Mechanical and Aerospace Engineering Dept., MAE Rept. 1651, Princeton Univ., Princeton, NJ, 1983.

[11]Martinelli, L., "Calculation of Viscous Flows with a Multi-Grid Method," Ph.D. Dissertation, Princeton Univ., Princeton, NJ, 1987.

[12]Baldwin, B. S., and Lomax, H., "Thin Layer Approximation and Algebraic Model for Separated Turbulence Flows," AIAA Paper 78-257, Jan. 1978.

[13]Mayle, R. E., "The Role of Laminar-Turbulent Transition in Gas Turbine Engines," *Journal of Turbomachinery*, Vol. 113, Oct. 1991, pp. 509–537.

[14]Abernathy, R. B., and Benedict, R. P., "Measurement Uncertainty: A Standard Methodology," Instrument Society of America, Research Triangle Park, NC, 1984.